N94-34197

PARAMETER IDENTIFICATION OF A ROTOR SUPPORTED IN A PRESSURIZED BEARING LUBRICATED WITH WATER

John W. Grant, Agnes Muszynska, and Donald E. Bently
Bently Rotor Dynamics Research Corporation
Minden, Nevada

ABSTRACT

A rig for testing an externally pressurized (hydrostatic), water—lubricated bearing was developed. Applying a nonsynchronous sweep frequency, rotating perturbation force with a constant amplitude as an input, rotor vibration response data was acquired in Bode and Dynamic Stiffness formats. Using this data, the parameters of the rotor/bearing system were identified. The rotor/bearing model was represented by the generalized (modal) parameters of the first lateral mode, with the rotational character of the fluid force taken into account.

1. INTRODUCTION

Experimental modal testing is a popular method for studying vibration problems of mechanical structures. The application of modal testing to a structure containing rotating elements requires a specialized approach [1]. The experimental testing provides data for identification of the system parameters which can be further used in the evaluation to the stability of the system, and in numerical modelling or engineer assist (expert system) programs. This paper presents results of perturbation testing and parameter identification of a rotor supported in one rigid and one externally pressurized water—lubricated bearing. The mathematical model used for the rotor system identification was developed in references [1—11]. The method of relating the applied input force to measured output response (henceforth known as the dynamic stiffness technique) serves very well for the parameter identification [1]. A new tool was developed for the experimental testing of the rotor/bearing system. This tool consists of a constant force amplitude perturbator used to apply the force to the system under test over a frequency range of ±3000 rpm (perturbation forward and backward). The unique feature of this perturbator is that the force has a constant amplitude, independent of frequency, unlike that of unbalance type perturbation. This feature enables one to obtain very clean (high signal to noise ratio) data in the low frequency range, therefore, it offers more accurate identification of the lowest modes of rotors with fluid interaction.

2. EXPERIMENTAL TEST RIG

The experimental rotor is shown in Figure 1. The system consists of a stainless steel shaft carrying a balanced, concentrated mass at the brass—sleeved, aluminum journal of 1.990 inch diameter and 10 mil diametrical clearance inside the bearing. The shaft is supported on one end by a relatively rigid, bronze (oilite) bearing, and the other by the water—lubricated, hydrostatic bearing. This cylindrical bearing has four equally spaced, canoe—shaped pockets, as shown in Figure 2. These pockets are fed through radial 0.135 inch diameter capillaries. The bearing contains, also, separately controlled tangential antiswirl ports. They will not be used, however, in the tests presented in this paper. The role of these ports is described in [12].

PRECEDING PAGE BLANK NOT FILMED

PAGE 372 INTENTIONALLY BLANK

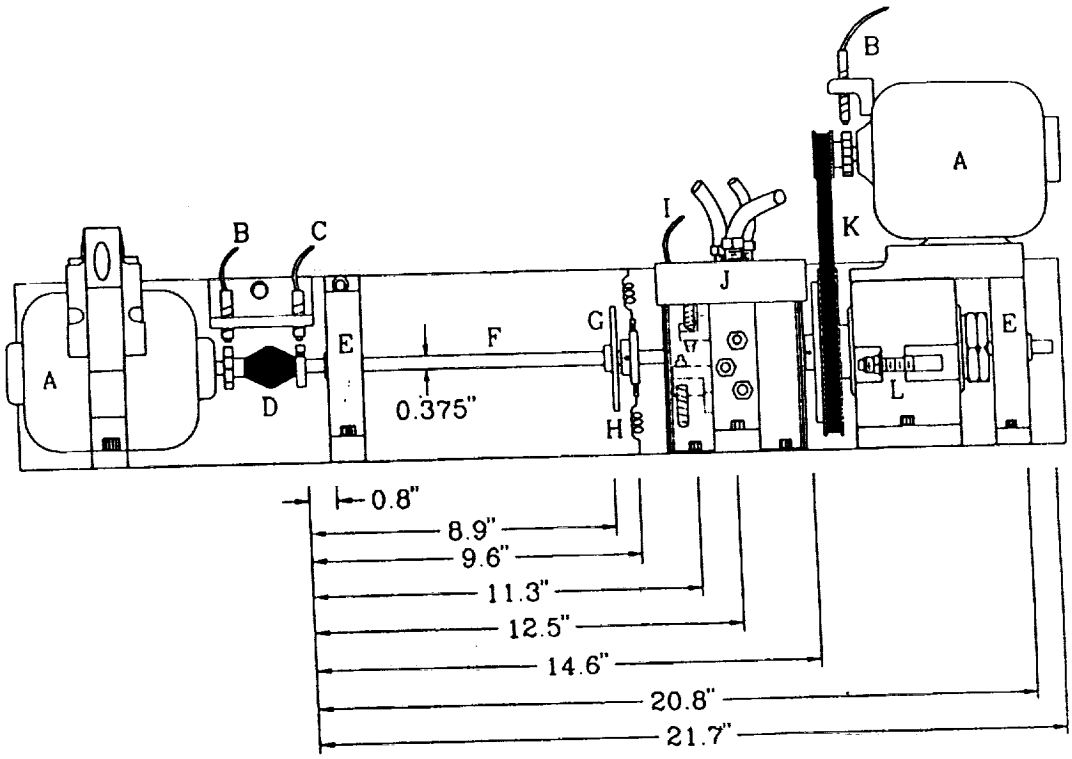

Fig. 1 Experimental rotor rig with constant force perturbator, A) 0.5 hp electric motor, B) speed control probe, C) Keyphasor® probe, D) flexible coupling, E) bronze sliding bearing, F) shaft, G) slim disk for balancing, H) spring support (with stiffness 38 lb/in), I) XY eddy current displacement probes, J) experimental pressurized bearing, K) constant force perturbator, L) optical Keyphasor.

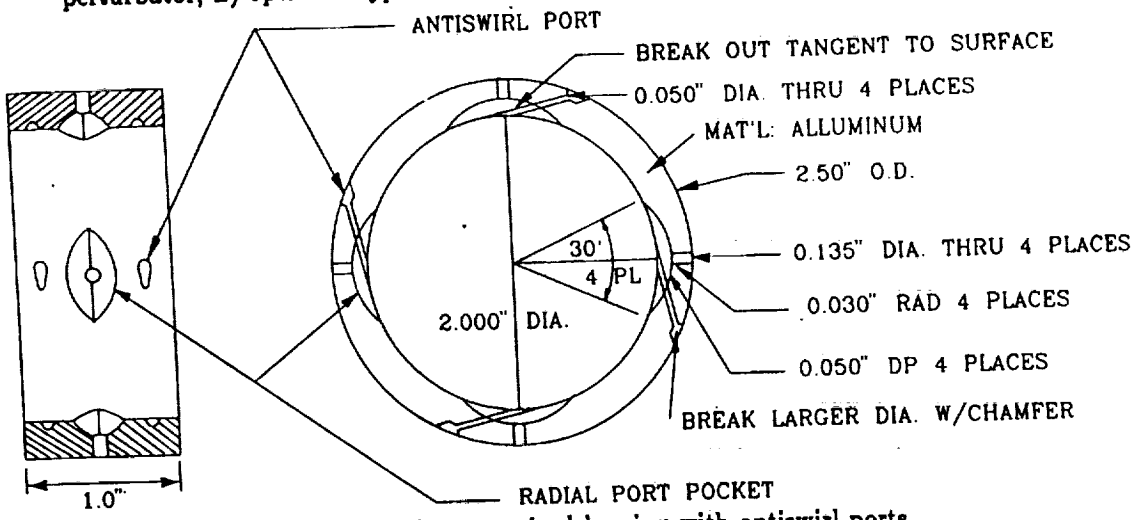

Fig. 2 Externally pressurised bearing with antiswirl ports.

The water temperature was monitored using a thermocouple that was located in a drain tube of the hydrostatic bearing. The rotative energy was derived from a 0.5 hp electric motor connected to the rotor through a flexible coupling. A speed controller was used to control rotative speed. The perturbation force was applied to the shaft rotating at a constant speed. Soft supporting springs installed near the test bearing allow for controlling journal eccentricity at rest: all tests were run with the journal concentrically located within the bearing. To obtain the shaft/journal lateral vibration data, one pair of XY eddy current displacement probes was mounted to

observe the shaft, next to the journal. A computerized data acquisition and processing system was used in the tests.

The right side of Figure 1 presents the system used to perturb the rotor/bearing system. The system consists of a stiff steel shaft connected to the journal within the hydrostatic bearing, using a sealed rolling element bearing. The shaft was supported on the other end by a bronze (oilite) bearing. A constant force perturbator was attached to the shaft next to the journal through a rolling element bearing (Fig. 3). The rotative energy for the perturbation was derived from a 0.5 hp bidirectional electric motor. Another speed controller was used to control perturbation speed and acceleration. The rotor response, to the input perturbation force, was filtered to the perturbation frequency. The response phase was measured in reference to an optical Keyphasor® that observed a reflective spot on the perturbator.

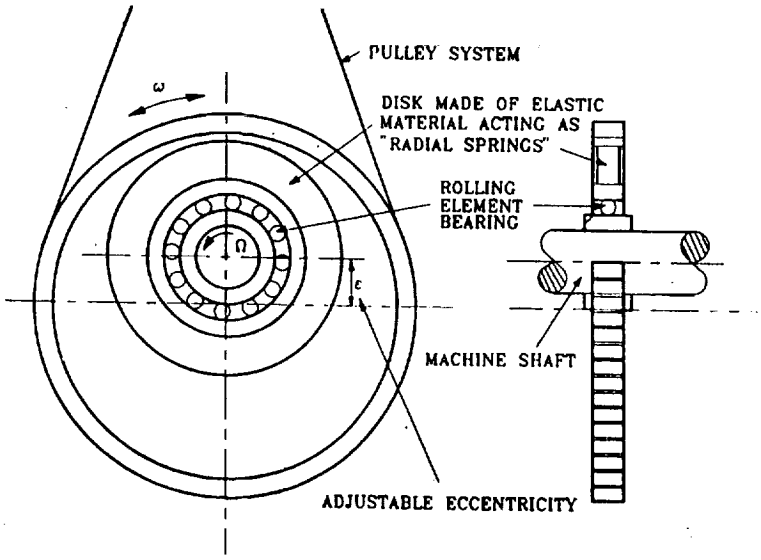

Fig. 3 Constant force perturbator (not to scale; eccentricity ϵ exaggerated).

3. CONSTANT FORCE AMPLITUDE PERTURBATOR

In previous experiments [1—12] the input perturbation force applied to the rotor was generated by an unbalance. Since unbalance centrifugal force is proportional to rotative speed squared, its amplitude becomes very small for low perturbation frequencies. A new device was designed that provides a constant force amplitude in order to increase the data accuracy in the low frequency range. The principle of the operation of this force perturbator is similar to the kinematic excitation, known in vibration theory: a calibrated rotating vector of displacement (ϵ) is exerted across a known radial stiffness (K) of the elastic material within the perturbator. This creates a known rotating force vector that is applied to the rotor under test. The known displacement is obtained by adjusting the eccentricity of an inner calibrated ring, as shown in Figure 3. To obtain the rotating force sweep frequency, the perturbation disk is rotated with very low acceleration in a direction the same as the rotor under test (forward perturbation), or opposite the direction (reverse perturbation). The elastic material used for the perturbator was Dow Corning® 3112 RTV silicon rubber. The stiffness, damping, and inertia of this material were separately identified by the use of dynamic stiffness testing of the perturbator itself. It was found that maximum inertia effect was 0.000209 lb sec^2/inch and maximum damping was 0.079 lb sec/inch. Using both static and dynamic testing, the perturbator radial stiffness was evaluated to be 374 lb sec/inch, as shown in Figure 4. Since the inertia and damping proved to be small compared to the stiffness, they were eventually neglected in the input force model.

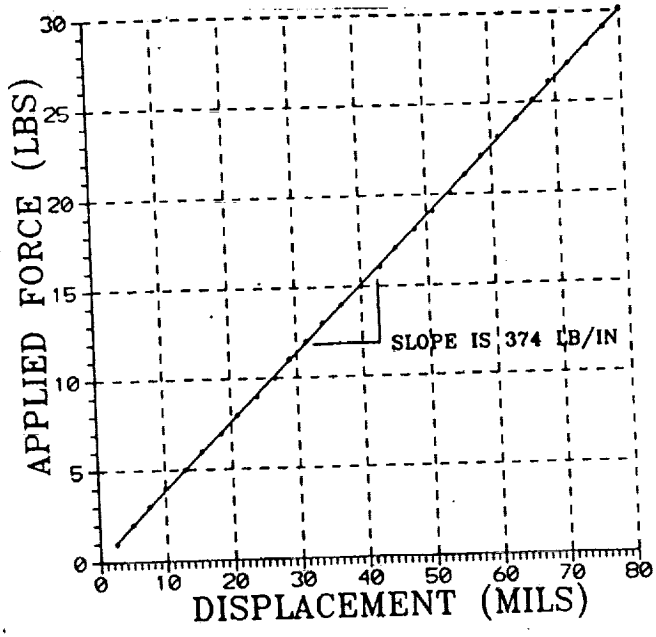

Fig. 4 Perturbator disk radial stiffness. Results from static tests.

4. WATER DELIVERY SYSTEM

To study hydrostatic bearing/seals, a high pressure water system (1000 psi @ 10 gpm) was developed. It consists of a 50 gallon water storage drum, low—pressure feed pump (100 psi), high—pressure multistage centrifugal pump (400 psi) driven by a 5 hp, 3 phase, 230 volt electric motor rotating at 3450 rpm. This delivers water through a pipeline which contains 80 mesh, 25 micron, and 1 micron filters, and several gauges and valves. Water is returned to the 50 gallon storage drum using a sump pump. Water temperature is openly controlled by using a submersion heater in the storage tank, with cooling provided by a fan blowing air at the storage tank surface.

The water is delivered to the hydrostatic bearing using three specially designed distribution manifolds. One manifold leads to the four radial ports, and the other two to the eight antiswirl ports of the test bearing. Each port is fed from the manifold to the port through a manually controlled flow valve, and a high—pressure hose. Each of the high—pressure feed lines is equipped with pressure gauges to measure the pressure drop at the bearing port. Pressure is also monitored at the manifold.

Flow is measured using the sump pump. The sump holds a calibrated 2.5 gallons before pumping, thus by timing this volume, the total flow rate is determined. Such calculation is only valid when testing one set of ports at a time, and when the journal rotates concentrically within the bearing.

5. MATHEMATICAL MODEL

The mathematical model of the fluid dynamic force and the corresponding dynamic stiffness components of the rotor/bearing system were developed in [1,3].

The model of the considered system is as follows:

$$M\ddot{z} + M_f(\ddot{z} - 2j\lambda\Omega\dot{z} - \lambda^2\Omega^2 z) + D(\dot{z} - j\lambda\Omega z) + (K_S + K_B + K)z = K\epsilon e^{j(\omega t+\delta)} \quad , \quad j=\sqrt{-1}$$

where $z = x+jy$ is the rotor lateral (x = horizontal, y = vertical) displacement, K_S and M are the rotor modal stiffness and mass, M_f is the fluid inertia effect, K_B and D are the fluid radial stiffness and damping respectively, and λ is the fluid average circumferential velocity ratio (the rate at which the fluid damping force rotates), with ω and Ω being perturbation frequency and rotative speed, respectively. K is the perturbator radial stiffness, ε and δ are the perturbator calibrated eccentricity parameters: its value and angular orientation, respectively. The rotor response is $z = Ae^{j(\omega t+\alpha)}$ where A and α are amplitude and phase respectively. The following relationships were further used in the identification procedure:

$$\text{Direct Dynamic Stiffness} = K_S+K_B+K-M_f(\omega-\lambda\Omega)^2 - M\omega^2 = \frac{K\varepsilon}{A}\cos(\delta-\alpha) \quad (1)$$

$$\text{Quadrature Dynamic Stiffness} = D(\omega-\lambda\Omega) = \frac{K\varepsilon}{A}\sin(\delta-\alpha) \quad (2)$$

Since Eqs. (1) and (2) are simple curves with respect to the perturbation frequency, it was possible to identify the parameters by using polynomial best fitting. The coefficients of the polynomial for these best fit curves can then be equated to the corresponding coefficients in Eqs. (1) and (2) to determine the value of each parameter.

6. EXPERIMENTAL TEST RESULTS

The set of tests was designed to determine the effects of pressurized water input through the radial inlets to the bearing (antiswirl ports shut off). The pressure at the radial port manifold was approximately 75 psi, and the drop across the bearing through the pocket was maintained constant at 20 psi. The water flow through the bearing varied from 3.9 to 4.6 gal/min for four consecutive tests. During four consecutive tests, the rotative speed was constant 0, 1000, 2000, and 3000 rpm respectively.

Figure 5 shows the rotor responses to a rotating sweep frequency perturbation force vector of $\varepsilon K = 1.535$ lbs at $\delta = -310°$. The responses to perturbation forward $(+\omega)$ and backward $(-\omega)$ were filtered to the perturbation frequencies and are presented in the Bode format (Fig. 5). Notice that the response amplitudes in the considered range of frequencies are rather flat, not the same as if the system was excited by an unbalance force. Note, also, that there is some disturbance in amplitudes and phases around the area when the perturbation and rotation frequency are equal. This is due to an interference of the rotative frequency vibrations in the filtering system.

Figure 6 presents the dynamic stiffness plots that were obtained using Eqs. (1) and (2), and the rotor response shown in Figure 5. Each plot consists of 570 data points. To identify the system's modal parameters, the plots were best fitted by polynomials. Interesting enough, the coefficients of higher power than the second for the direct stiffness, and first for the quadrature stiffness, were more than five orders smaller than those of lower powers. Therefore, a parabola was adopted for the direct, and a straight line for the quadrature dynamic stiffness. They are shown as solid lines in the plots of Figure 6. The coefficients of the best fit equations are summarized in Table 1.

If the best fit coefficients are equated to that of the dynamic stiffness model (1), (2), and converted to the proper angular frequency units, the system parameters can be identified, as shown in Table 2.

When calculating the rotor modal mass M at rotative speed of 0 rpm, the fluid inertia effect and the mass cannot be readily separated ($M_f + M = 7.37 \times 10^{-3}$). To obtain reasonable data for zero speed, the modal mass was obtained by averaging the values at all other rotative speeds.

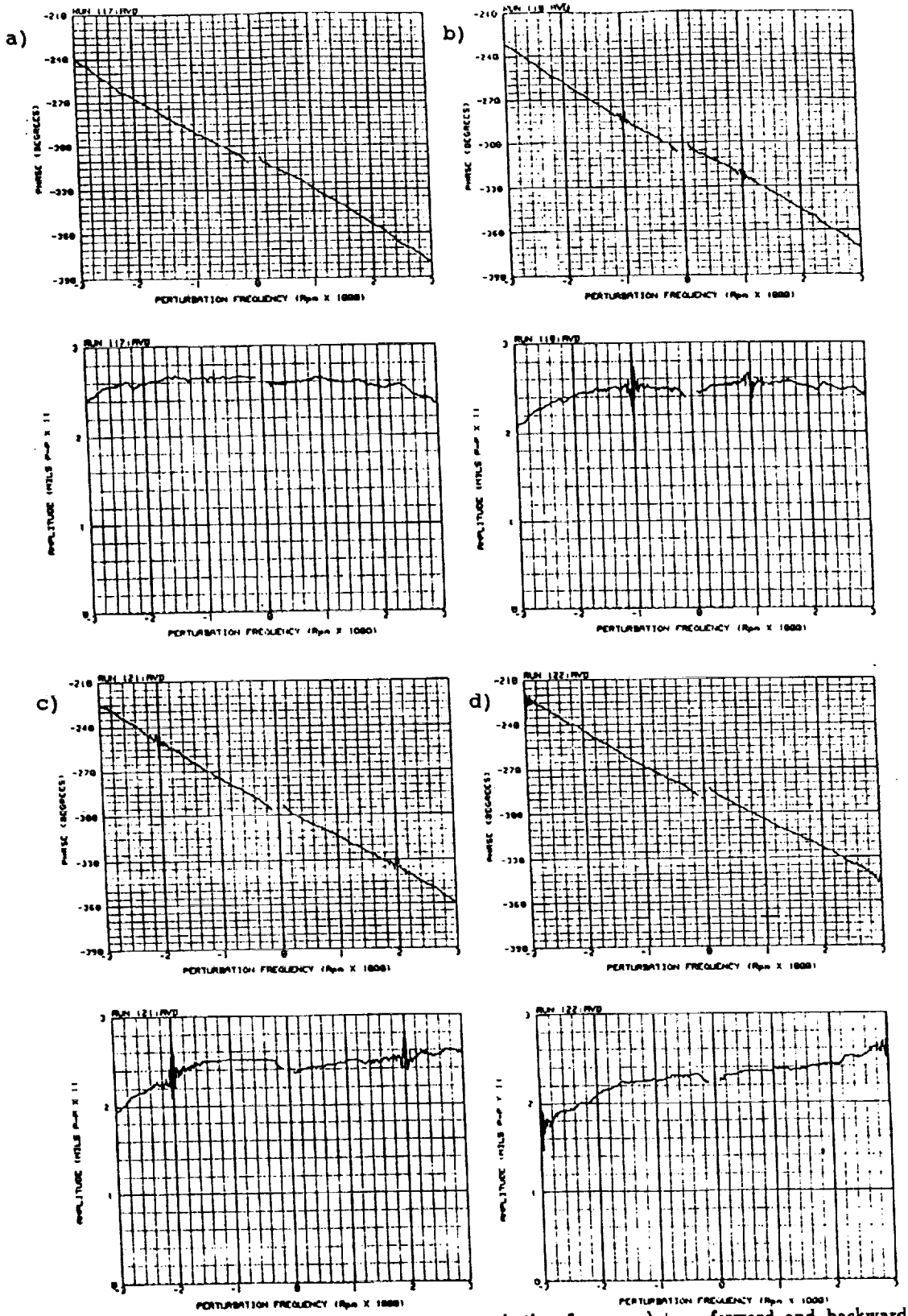

Fig. 5 Rotor vertical response (filtered to perturbation frequency) to a forward and backward perturbation force rotating vector of $K\epsilon$ = 1.535 lbs at δ = -310°, with the water-lubricated bearing radial port pocket pressure of 20 psi and a rotative speed of (a) 0 rpm, (b) 1000 rpm, (c) 2000 rpm, and (d) 3000 rpm. The horizontal responses which were very similar are not shown. Response amplitude measured peak to peak.

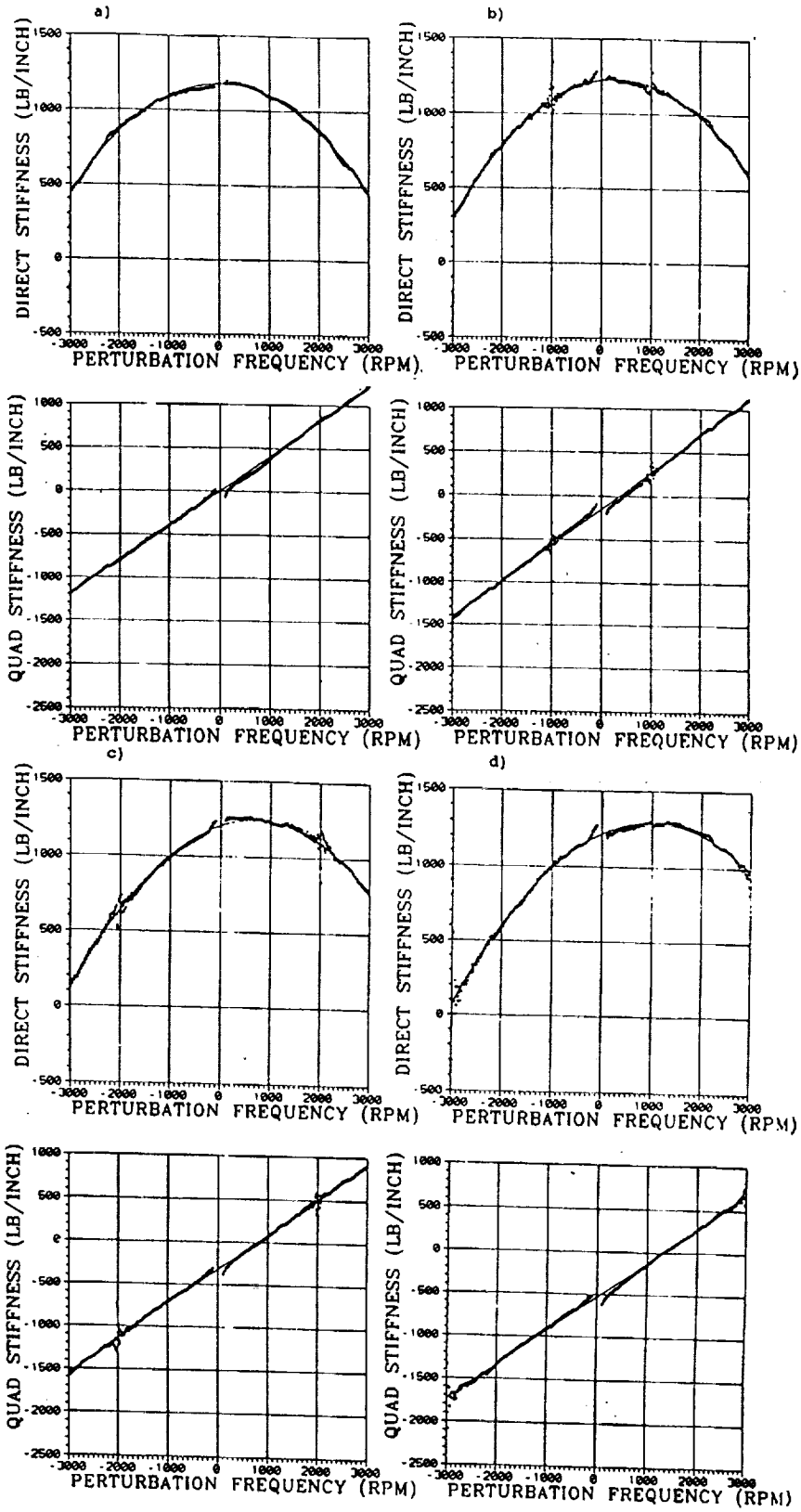

Fig. 6 Direct and quadrature dynamic stiffness plots based on Eqs. (1), (2) and on the system responses presented in Figure 5 for four rotative speeds: (a) 0 rpm, (b) 1000 rpm, (c) 2000 rpm, and (d) 3000 rpm.

C5.

Table 1. Best Fit Coefficients of the Polynomials in Fig. 6

Rotative Speed Ω	Direct Dynamic Stiffness $A+B\omega+C\omega^2$			Quadrature Dynamic Stiffness $E\omega+F$	
rpm	A	$B\times10^{-3}$	$C\times10^{-5}$	E	F
0	1182	2.126	-8.084	0.400	3.424
1000	1226	49.30	-8.557	0.420	-150.5
2000	1205	113.6	-8.363	0.408	-318.9
3000	1220	152.0	-7.707	0.402	-530.2

Table 2. Identified Parameters of the Rotor/Bearing System

Rotative Speed, Ω		D		λ	M_f		$K+K_s+K_B$		M	
rpm	$\frac{rad}{sec}$	$\frac{lb\times sec}{inch}$	$\frac{kg}{sec}$	---	$\frac{lb\times sec^2}{inch}\times10^{-3}$	kg	$\frac{lb}{inch}$	$\frac{N}{m}\times10^3$	$\frac{lb\times sec^2}{inch}\times10^{-3}$	kg
0	0	3.82	669	—	5.94	1.04	1182	207	1.43*	0.251*
1000	105	4.01	702	0.358	6.28	1.10	1235	216	1.52	0.267
2000	209	3.90	683	0.390	6.64	1.16	1249	219	0.99	0.173
3000	314	3.83	671	0.440	5.25	0.92	1320	231	1.78	0.312

*Average of the column

The average mass, $M_{avg} = 1.43 \times 10^{-3}$ lb sec^2/inch (0.251 kg), was then subtracted from the second order coefficient C, providing the fluid inertia effect value at 0 rpm.

As it was mentioned in reference [2], there is a possibility that the fluid radial damping and fluid inertia forces rotate at different rates of λ. A method to determine the fluid inertia rotation rate, λ_f, is to solve the equation resulting from equating Eq. (1) with the best fit coefficients and solve it for $M_f\lambda_f$ (see Table 1 and Eq. (1)):

$$M_f\lambda_f = \frac{B}{2\Omega}\left[\frac{30}{\pi}\right]^2 \tag{3}$$

where B is the first order coefficient of the direct stiffness best fit parabolas (Table 1). If the average modal mass, M_{avg}, is used again, the fluid inertia effect can be calculated from the second order coefficient of the parabola:

$$M_f = -\left[C\,(\frac{30}{\pi})^2 + M_{avg}\right] \tag{4}$$

where C is the second order coefficient of the direct dynamic stiffness best fit parabola (Table 1). The ratio λ_f is calculated by dividing Eq. (3) by Eq. (4). The results are summarized in Table 3. They show that the values λ and λ_f are, actually, very close (maximum difference is 7.2%).

Table 3. Identification of the Fluid Inertia Average Circumferential Velocity Ratio

Rotative Speed Ω		$M_f\lambda$		M_f		λ_f
rpm	$\frac{\text{rad}}{\text{sec}}$	$\frac{\text{lb}\times\text{sec}^2}{\text{inch}}$ $\times 10^{-3}$	kg	$\frac{\text{lb}\times\text{sec}}{\text{inch}}$ $\times 10^{-3}$	kg	---
1000	105	2.25	0.394	6.37	1.12	0.353
2000	209	2.59	0.454	6.19	1.08	0.418
3000	314	2.31	0.405	5.60	0.98	0.413

Figure 7 presents the results from another set of perturbation tests in which the rotative speed varied, while the perturbation force was constant with $K\varepsilon = 1.535$ lbs and $\delta = -310°$. The quadrature dynamic stiffness data were identified as parabolas or straight lines by best fitting polynomials (Table 4). The corresponding quadrature stiffness components D and λ that were calculated from the data are summarized in Table 5. Generally, D resulting from these tests is slightly higher, and λ slightly lower than obtained from the previous tests.

All test results were not compensated for the water temperature changes, which, within each test, varied from 0.3° F to 0.8° F within the range of 90.4° F to 96° F. The data acquisition system was set on the average value of the proximity transducer sensitivity, 0.2 v/mil. Due to slightly increasing temperature during the tests, the transducer output sensitivity varied from 0.198 v/mil to 0.199 v/mil, thus the amplitude readings were 0.5% to 1% higher than the actual ones, and, consequently, the dynamic stiffness values became from 0.5% to 1% lower.

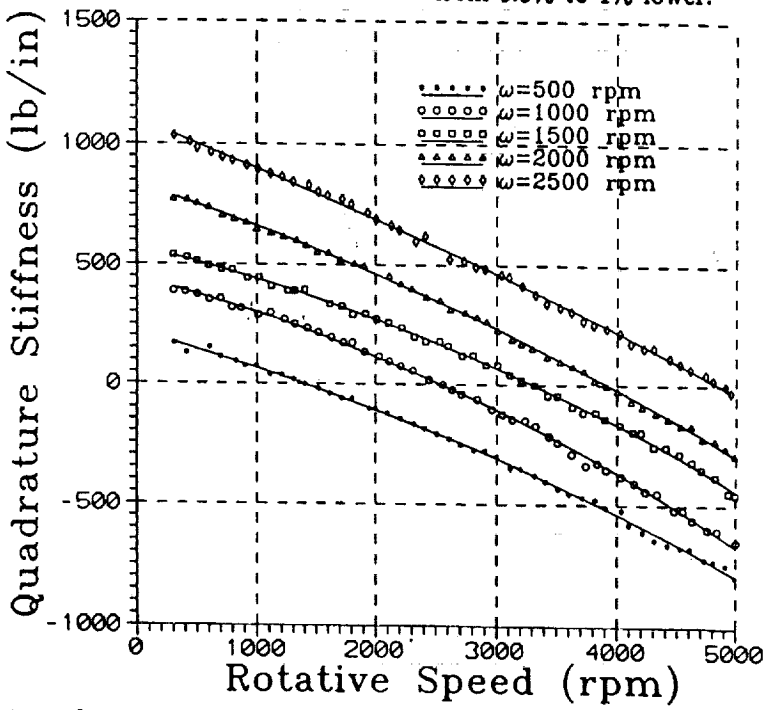

Fig. 7 Quadrature dynamic stiffness versus rotative speed for constant values of perturbation frequency. The solid lines are best fits using second order polynomials.

Table 4. Best Fit Coefficients for the Polynomials of the Quadrature Dynamic Stiffness From Fig. 6 Versus Rotative Speed.

Perturbation Speed ω, rpm	Second Order Fit $G+H\Omega+I\Omega^2$			First Order Fit $J\Omega+L$	
	G	$H\times10^{-3}$	$I\times10^{-6}$	$J\times10^{-3}$	L
500	216	-136	-13	-207	287
1000	443	-123	-19	-228	543
1500	573	-115	-17	-208	662
2000	835	-159	-13	-231	904
2500	1097	-188	-8	-229	1137

Table 5. Identified Parameters for Quadrature Dynamic Stiffness Using Eq. (2) and Polynomial Fits From Table 4.

Perturbation Speed, ω		Second Order Fit Parameters			First Order Fit Parameters		
		D		λ	D		λ
rpm	rad/sec	lb * sec/inch	kg/sec	- - -	lb * sec/inch	kg/sec	- - -
500	52	4.13	723	0.315	5.47	958	0.361
1000	105	4.23	741	0.278	5.18	907	0.420
1500	157	3.64	637	0.301	4.22	739	0.471
2000	209	3.99	699	0.381	4.31	755	0.511
2500	262	4.19	734	0.429	4.34	760	0.504

The fluid radial damping calculated using the well–known formula: $D = \pi\eta r(\ell/c)^3$ (where η is fluid dynamic viscosity, r, ℓ and c are bearing radius, length, and radial clearance respectively) provides the values from 3.45 lb sec/inch to 3.22 lb sec/inch for water temperatures from 90.4° F to 96.5° F and corresponding viscosities varying from 0.7577 c poise to 0.7076 c poise through the entire set of tests. The identified values of D were, therefore, lower than the calculated ones. The proper temperature compensation of the results would decrease the difference.

7. CONCLUSIONS

Developed over two years ago, the high–pressure water rotor rig can be used for dynamic testing of bearing and seals. This paper presented test results of an externally pressurized bearing for only one pressure value. Applying the nonsynchronous perturbation testing which has been extensively used by the authors through the last 12 years, the fluid force parameters were identified. The results confirm, again, the meaningfulness of the fluid circumferential average velocity ratio as the important element of the fluid force model in lightly loaded lubricated bearings and seals. The results also indicate the existence of the fluid inertia effect which is relatively high, about five times larger than the rotor modal mass.

The use of the constant force perturbator has enabled the acquisition of very clean vibration data (higher signal, thus better signal to noise ratio) in the low frequency range, and hence clean dynamic stiffness data was produced. This data makes the identification procedure more accurate, and allows for advancements in adjustments of the mathematical model of the rotor/bearing system.

NOMENCLATURE

A,B,C,E,F,G,H,I,J,L	Best fit polynomial coefficients
A,α	Rotor response amplitude and phase respectively
D,K_B,M_f	Fluid radial damping, radial stiffness, and inertia effect respectively
$j=\sqrt{-1}$	
K_s,M	Rotor modal stiffness and mass respectively
K	Perturbator radial stiffness
$z=x+jy$	Rotor lateral (x=horizontal, y=vertical) displacement
δ,ϵ	Perturbator angular orientation and eccentricity respectively
λ	Fluid circumferential average velocity ratio at which fluid damping force rotates
λ_f	Ratio of the fluid inertia force rotation
ω	Perturbation frequency
Ω	Rotative speed

REFERENCES

1. Muszynska, A., Perturbation Technique for Identification of the Lowest Modes of Rotors With Fluid Interaction, Course on "Rotor Dynamics and Vibration in Turbomachinery," von Karman Institute for Fluid Dynamics, Belgium, 21—25 September 1992.

2. Muszynska, A., Bently, D. E., Frequency Swept Rotating Input Perturbation Techniques and Identification of the Fluid Force Models in Rotor/Bearing Seal Systems and Fluid Handling Machines, Journal of Sound and Vibration, v. 143, No. 1, pp. 103—124, 1990.

3. Muszynska, A., Improvements in Lightly Loaded Rotor/Bearing and Rotor/Seal Models, Transaction of the ASME Journal of Vibration Acoustics, Stress and Reliability in Design, v. 110, No. 2, April 1988.

4. Muszynska, A., Whirl and Whip — Rotor/Bearing Stability Problems, Journal of Sound and Vibration, v. 110, No. 3, 1986.

5. Bently, D. E., Muszynska, A., Stability Evaluation of Rotor/Bearing System by Perturbation Tests, Rotor Dynamic Instability Problems in High Performance Turbomachinery, NASA CP 2250, The Second Workshop at Texas A&M University, College Station, Texas, 1982.

6. Bently, D. E., Muszynska, A., Oil Whirl Identification by Perturbation Test, Advances in Computer—Aided Bearing Design, 82—72978, ASME/ASLE Lubrication Conference, Washington, D.C., October 1982.

7. Bently, D. E., Muszynska, A., Perturbation Tests of Bearing/Seal for Evaluation of Dynamic Coefficients, Symposium on Rotor Dynamical Instability, Summer Annual Conference of the ASME Applied Mechanics Division, AMD — Vol. 55, Houston, Texas, June 1983.

8. Bently, D. E., Muszynska, A., Perturbation Study of Rotor/Bearing System: Identification of the Oil Whirl and Oil Whip Resonances, Tenth Biennial ASME Design Engineering Division Conference on Mechanical Vibration and Noise, 85—DET—142, Cincinnati, Ohio, September 1985.

9. Bently, D. E., Muszynska, A., Modal Testing and Parameter Identification of Rotating Shaft/Fluid Lubricated Bearing System, Proc. of the 4th International Modal Analysis Conference, Los Angeles, California, February 1986.

10. Muszynska, A., Grant, J. W., Stability and Instability of a Two—Mode Rotor Supported by Two Fluid—Lubricated Bearings, Trans. of the ASME Journal of Vibration and Acoustics, v. 113, No. 3, 1991.

11. Bently, D. E., Muszynska, A., Role of Circumferential Flow in the Stability of Fluid—Handling Machine Rotors, Texas A&M Fifth Workshop on Rotordynamics Instability Problems in High Performance Turbomachinery, College Station, Texas, 16—18 May 1988.

12. Muszynska, A., Bently, D. E., Franklin, W. D., Grant, J. W., Goldman, P., Applications of Sweep Frequency Rotating Force Perturbation Methodology in Rotating Machinery for Dynamic Stiffness Identification, 92—GT—176, ASME International Gas Turbine and Aeroengine Congress and Exposition, Cologne, Germany, June 1992, Trans. of the ASME, Journal of Engineering for Gas Turbines and Power, April 1993.